



Short GRBs: Opening Angles, Local Neutron Star Merger Rate, and Off-axis Events for GRB/GW Association

Zhi-Ping Jin^{1,2} , Xiang Li¹, Hao Wang^{1,2} , Yuan-Zhu Wang^{1,2} , Hao-Ning He¹, Qiang Yuan^{1,2}, Fu-Wen Zhang³ ,
Yuan-Chuan Zou⁴ , Yi-Zhong Fan^{1,2} , and Da-Ming Wei^{1,2}

¹ Key Laboratory of dark Matter and Space Astronomy, Purple Mountain Observatory, Chinese Academy of Science, Nanjing, 210008, People's Republic of China
yzfan@pmo.ac.cn, dmwei@pmo.ac.cn, jin@pmo.ac.cn

² School of Astronomy and Space Science, University of Science and Technology of China, Hefei, Anhui 230026, People's Republic of China

³ College of Science, Guilin University of Technology, Guilin 541004, People's Republic of China

⁴ School of Physics, Huazhong University of Science and Technology, Wuhan 430074, People's Republic of China

Received 2017 August 28; revised 2018 February 25; accepted 2018 March 14; published 2018 April 24

Abstract

The jet breaks in the afterglow light curves of short gamma-ray bursts (SGRBs), rarely detected so far, are crucial for estimating the half-opening angles of the ejecta (θ_j) and hence the neutron star merger rate. In this work, we report the detection of jet decline behaviors in GRB 150424A and GRB 160821B, and find $\theta_j \sim 0.1$ rad. Together with five events reported before 2015 and three others “identified” recently (GRB 050709, GRB 060614, and GRB 140903A), we have a sample consisting of nine SGRBs and one long-short GRB with reasonably estimated θ_j . In particular, three *Swift* bursts in the sample have redshifts $z \leq 0.2$, with which we estimate the local neutron star merger rate density to be $\sim 1109_{-657}^{+1432} \text{ Gpc}^{-3} \text{ yr}^{-1}$ or $162_{-83}^{+140} \text{ Gpc}^{-3} \text{ yr}^{-1}$ if the narrowly beamed GRB 061201 is excluded. Inspired by the typical $\theta_j \sim 0.1$ rad found currently, we further investigate whether the off-beam GRBs (in the uniform jet model) or the off-axis events (in the structured jet model) can significantly enhance the GRB/GW association. For the former, the enhancement is at most moderate, while for the latter the enhancement can be much greater and a high GRB/GW association probability of $\sim 10\%$ is possible. We also show that the data of GRB 160821B may contain a macronova/kilonova emission component with a temperature of ~ 3100 K at ~ 3.6 days after the burst and more data are needed to ultimately clarify.

Key words: binaries: close – gamma-ray burst: individual (GRB 150424A, GRB 160821B) – gravitational waves

1. Introduction

Gamma-ray bursts (GRBs) are brief, intense, gamma-ray flashes that are widely believed to be powered by the dying massive stars (also called collapsars) or the merging of the compact binaries involving at least one neutron star (see Piran 2004; Kumar & Zhang 2015, for reviews). Bright supernova (SN) emissions have been detected in the late afterglows of some low-redshift long-duration GRBs (LGRBs, i.e., GRBs with durations longer than 2 s), established their collapsar origin (Woosley & Bloom 2006). The neutron star merger model is more likely relevant to short GRBs (SGRBs), the events with durations shorter than 2 s (Eichler et al. 1989; Kouveliotou et al. 1993). The direct evidence for the merger origin of SGRBs was absent until 2017 August 16, due to the non-detection of SGRB/GW association. There was, however, some indirect evidence for SGRBs originating from compact binaries, including the location of SGRBs in elliptical galaxies; non-detection of associated SN; large galaxy offsets; weak spatial correlation of SGRBs and star formation regions within their host galaxies (see Nakar 2007; Berger 2014, for reviews); and in particular, the identification of the so-called Li-Paczynski macronovae in GRB 130603B (Berger et al. 2013; Tanvir et al. 2013), GRB 060614 (Jin et al. 2015; Yang et al. 2015) and GRB 050709 (Jin et al. 2016). The Li-Paczynski macronova (also called a kilonova) is a new kind of near-infrared/optical transient, powered by the radioactive decay of r -process material, which is synthesized in the ejecta launched during the merger event (e.g., Li & Paczyński 1998; Kulkarni 2005; Metzger et al. 2010; Barnes & Kasen 2013; Hotokezaka et al. 2013; Tanaka & Hotokezaka 2013). On the other hand, the mergers of compact binaries consisting of neutron stars

(NSs) and/or black holes (BHs) are promising sources of gravitational waves (GW; Clark & Eardley 1977). Therefore, SGRBs are expected to be one of the most important electromagnetic counterparts of the GW events (e.g., Eichler et al. 1989; Kochanek & Piran 1993; Li et al. 2016; Baiotti & Rezzolla 2017; Paschalidis 2017). The successful detection of GW170817/GRB 170817A/AT2017gfo (Abbott et al. 2017; Coulter et al. 2017; Goldstein et al. 2017; Pian et al. 2017), reported during the revision of this work, directly confirms all of the above opinions/speculations.

The SGRB data had been widely used to estimate the rate of neutron star mergers, hence the detection prospect of the GW detectors (e.g., Guetta & Piran 2005; Nakar 2007; Abadie et al. 2010; Coward et al. 2012; Fong & Berger 2013; Fong et al. 2014; Li et al. 2017). Such an approach is still necessary after the successful detection of GW170817. This is because although the mergers of double neutron stars (neutron star-black hole binaries) can be directly measured by advanced LIGO/Virgo, the horizon distances of detecting such events by the second-generation detectors are limited to be $z < 0.1$ (0.2), even under a optimistic situation (for example, the successful detection of the electromagnetic counterparts). Therefore, at relatively higher redshifts, the SGRB data are valuable in estimating the neutron star merger rate. At low redshifts, the comparison of the geometry-corrected SGRB rate with the directly measured neutron star merger rate can be used to evaluate the probability of launching relativistic outflow in these mergers. For such purposes, the half-opening angles of the SGRB ejecta are crucial. In principle, the half-opening angle of GRB ejecta can be reasonably estimated with the measured jet break in the afterglow light curve (Rhoads 1999;

Sari et al. 1999). Such jet breaks are, unfortunately, only rarely detected for SGRBs. As summarized in Fong et al. (2015), previously there were just four SGRBs, including GRB 051221A, GRB 090426A, GRB 111020A, and GRB 130603B, with reliable jet-break measurements and hence the half-opening angle estimates (GRB 061201 with a sharp jet break displaying in the X-ray data (Stratta et al. 2007) was, however, ignored in such a summary). The deep X-ray measurement of GRB 140903A reveals a jet break at ~ 1 day after the burst (Troja et al. 2016a), suggesting a $\theta_j \sim 0.05$ – 0.1 rad (Zhang et al. 2017). The sample increases a bit further if we also include the jet break displaying in the so-called long-short GRB (lsGRB) 060614 (Xu et al. 2009; Jin et al. 2015) and the quick decline behavior needed in modeling of short GRB 050709 (Jin et al. 2016). Even so, the “enlarged” sample consists of just $< 7\%$ SGRBs, and it is unclear whether the majority of the SGRBs are beamed. One speculation is that the jet breaks usually take place very late, and deep follow-up observations are needed. The search for macronova/kilonova components in late time afterglow emission of SGRBs, motivated by the signal detected in GRB 130603B, provided such a chance. In this work, we analyzed the *Hubble Space Telescope* (*HST*) data of GRB 150424A (Tanvir et al. 2015) and GRB 160821B (Troja et al. 2016b) to search for the jet breaks as well as the macronova signals.

This work is organized as follows. In Section 2, we describe our data analysis of GRB 150424A and GRB 160821B, and identify the jet breaks (or, more exactly, the post-jet-break decline behavior). We also examine whether there is evidence for a macronova emission component in GRB 160821B, and estimate the neutron star merger rate density in the local universe. In Section 3, inspired by the narrow jets found in the current sample, we investigate whether the off-beam GRBs (in the uniform jet model, the line of sight is outside of the ejecta) or the off-axis events (in the structured jet model, the line of sight is outside of the narrow energetic core of the ejecta) can significantly contribute to the GRB/GW association. We summarize our results with some discussions in Section 4.

2. Data Analysis of GRB 150424A and GRB 160821B; Jet Breaks of SGRBs/lsGRB; and the Local Neutron Star Merger Rate

2.1. Observations and Data Analysis of GRB 150424A and GRB 160821B

SGRB 150424A was detected by the Burst Alert Telescope (BAT) on board the *Swift* satellite at 07:42:57 (UT) on 2015 April 24, (Beardmore et al. 2015). The BAT light curve is composed by a bright multi-peaked short episode (start from $T - 0.05$ to $T + 0.5$ s) and a very weak extended emission (lasted to about $T + 100$ s) (Barthelmy et al. 2015). Konus-Wind also detected a multi-peak short burst with a total duration of ~ 0.4 s (Golenetskii et al. 2015). At 1.6 hr after the trigger, the Keck telescope observed the field and found the optical afterglow (Perley & McConnell 2015). Marshall & Beardmore (2015) checked the earlier *Swift* UV Optical Telescope (UVOT) observations and also found the afterglow. The *HST* visited the burst site for three epochs within a month (PI: Nial Tanvir, *HST* proposal ID: 13830). Recently, Knust et al. (2017) reported the multi-wavelength observation data of GRB 150424A and interpreted the central engine as a magnetar. In this work, we focus on the late observations

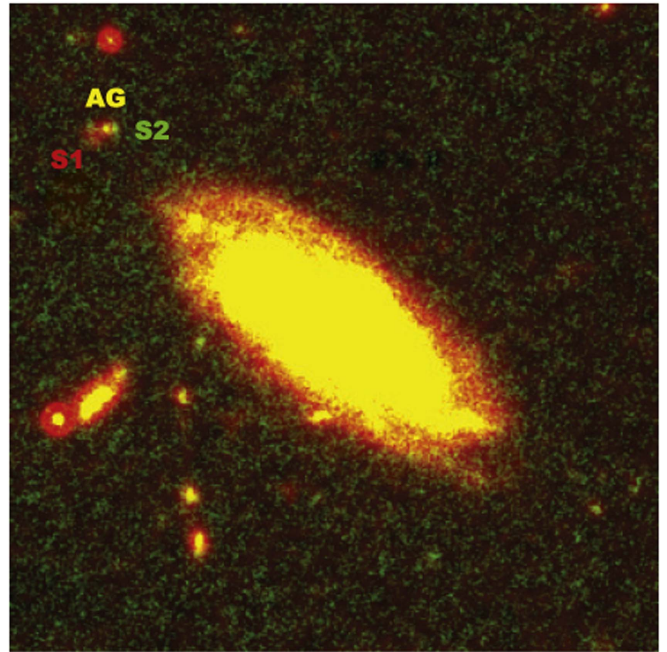


Figure 1. False color image of the field of GRB 150424A, which has been converted to north up and east left. Here, all *HST* WFC3 UVIS (including 2496 s in *F*435W, 7200 s in *F*606W, and 2496 s in *F*814W) signals appear in green, and all *HST* WFC3 IR (including 5395 s in *F*105W, 5991 s in *F*125W, and 5991 s in *F*160W) appear in red. The afterglow detected in both UV and IR images are marked as AG. There is a red source in the southeast only detected in IR images (marked as S1) and a blue source in the west only detected in UV images (marked as S2).

(> 0.5 day) to search for possible jet break and the macronova signal.

SGRB 160821B was detected by the *Swift* BAT at 22:29:13 (UT) on 2016 August 21, (Siegel et al. 2016). Its duration is $T_{90} = 0.48 \pm 0.07$ s. Following the BAT trigger, the X-ray telescope (XRT) and UVOT slew to the burst site immediately and started the observation in 66 and 76 s, respectively. The XRT found the afterglow at R.A. = 18:39:54.71 decl. = 62:23:31.3 (J2000) with an uncertainty of 2.5 arcseconds (Siegel et al. 2016). Based on the observation started at 0.548 hr after the burst, the Nordic Optical Telescope (NOT) first reported the detection of the optical afterglow at R.A. = 18:39:54.56 decl. = 62:23:30.5 (J2000) with an uncertainty of 0.2 arcsecond, and a host galaxy candidate that lies at about $5''.5$ away (Xu et al. 2016). Later, the William Herschel Telescope spectral observations of the host galaxy claimed a redshift of $z = 0.16$ based on the $H\alpha$, $H\beta$ and $O\text{ III } 4959/5007$ Å lines. The unambiguous classification as SGRB and the plausible low redshift make it an ideal candidate to search for a macronova. The *HST* visited the burst site for three epochs within a month (PI: Nial Tanvir, *HST* proposal ID: 14237).

Now the *HST* data of both GRB 150424A and GRB 160821B are publicly available, and we have downloaded these data from the Barbara A. Mikulski Archive for Space Telescopes (MAST: <http://archive.stsci.edu/>).

GRB 150424A was initially found near a bright spiral galaxy $R \sim 20$ mag (Perley & McConnell 2015) at a redshift of $z = 0.30$ (Castro-Tirado et al. 2015). The later deep *HST* observations, however, found that the field of GRB 150424A is very complicated (Tanvir et al. 2015). There is an extended source to the southeast of afterglow (see Figure 1, marked as S1) that is a candidate of the host galaxy of GRB 150424A,

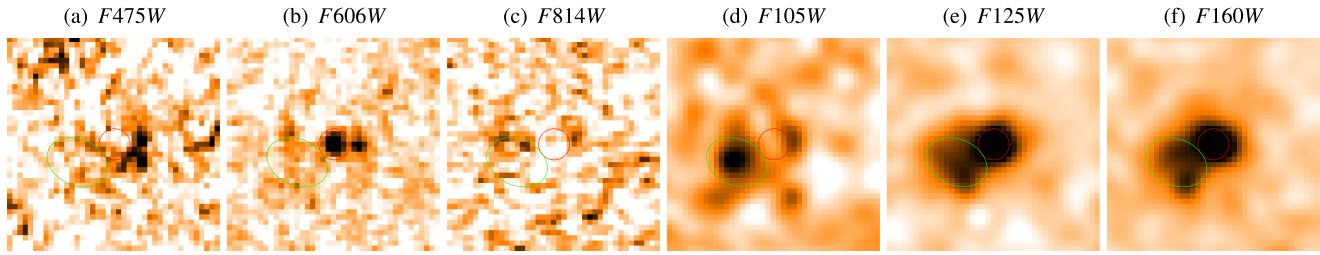


Figure 2. *HST* observations of GRB 150424A. Each image shows the combined data of all observations in the given filter. The red circle is the position of the afterglow and the green circle is the position of S1.

too. It has been detected in *HST* F105W, F125W, and F160W bands, but not in *HST* F475W, F606W, and F814W bands (see Figure 2). If the break between F105W and F814W is due to the 4000 Å break, then the redshift is $z \sim 1.2$. While the absence of strong evidence for a Lyman break in the *Swift* UVOT afterglow data (Marshall & Beardmore 2015; Knust et al. 2017) indicates a redshift of $z \leq 1.0$. Considering these uncertainties, we suggest that $z = 0.3$ is favored while $z \sim 1$ is still possible. The *HST* data of GRB 150424A have been analyzed by Knust et al. (2017) via a photometry with a $0''.4$ aperture. We have carried out an independent analysis of *HST* data using a slightly different method. We have adopted the image subtraction technique, taking all the observations at $t > 20$ days as the reference images, to remove the underlying sources (i.e., S1 and S2) from the afterglow emission. The afterglow is very weak in the second *HST* observation epoch. We have taken a three-pixels aperture for the photometry and then corrected to an infinite aperture. The results are reported in Table 1. Essentially, our results are in agreement with Knust et al. (2017), except that their photometry included the underlying sources S1 and S2, while we have removed them by image subtraction, hence our afterglow emission are weaker than Knust et al. (2017).

GRB 160821B is located near a bright ($R \sim 19.2$ mag) spiral galaxy (Xu et al. 2016), at a redshift of $z = 0.16$ (Levan et al. 2016). Deep *HST* observations found no secure detection of any underlying sources near the afterglow (see Figure 3). We then adopt $z = 0.16$ for this burst. For GRB 160821B, we have adopted a similar analysis method as GRB 150424A, including image subtraction, although there is no underlying source detected. The results are summarized in Table 2.

2.2. Identification of the Post-jet-break Decline Behaviors of GRB 150424A and GRB 160821B

In the GRB jet model (see Table 1 of Zhang & Mészáros (2004) for a comprehensive summary), the afterglow light curve declines as t^{-p} (or slightly shallower if the sideways expansion of the ejecta is ignorable), as long as the ejecta has been decelerated to a bulk Lorentz factor $\leq 1/\theta_j$, no matter whether the observer's frequency ν_{obs} is between ν_m and ν_c (the spectrum is $\propto \nu^{-(p-1)/2}$) or above both of them (the spectrum is $\propto \nu^{-p/2}$). Therefore, the quick decline $t^{-\alpha}$ at late time, together with a reliable spectral index that is close to $(\alpha - 1)/2$ or $\alpha/2$ for $\alpha \gtrsim 2$, are widely taken as strong evidence for the post-jet-break decline behavior.

For GRB 150424A, the F606W, F110W, and F160W data are consistent with the post-jet-break afterglow model for $p \sim 2.5$, for which the spectrum should be $\propto \nu^{-0.75}$ (for $\nu_m < \nu_{\text{obs}} < \nu_c$) and the decay should be $\propto t^{-2.5}$ (see Figures 4 and 5). Converting all bands to i' band with a spectrum of

Table 1
Observations of GRB 150424A

Time (days)	Exposure (s)	Instrument	Filter	Magnitude ^a (AB)
177.44649	2496	<i>HST</i> +WFC3	F475W	(>27.4) ^b
6.63693	1800	<i>HST</i> +WFC3	F606W	26.03 ± 0.06
9.22345	1800	<i>HST</i> +WFC3	F606W	26.98 ± 0.14
13.86864	1800	<i>HST</i> +WFC3	F606W	28.03 ± 0.37
178.47184	1800	<i>HST</i> +WFC3	F606W	(>28.2) ^b
177.51281	2496	<i>HST</i> +WFC3	F814W	(>26.9) ^b
177.61249	5395	<i>HST</i> +WFC3	F105W	(26.20 ± 0.11) ^b
6.67527	1498	<i>HST</i> +WFC3	F125W	25.25 ± 0.08
9.26352	1498	<i>HST</i> +WFC3	F125W	26.32 ± 0.21
13.92497	1498	<i>HST</i> +WFC3	F125W	27.08 ± 0.42
178.51300	1498	<i>HST</i> +WFC3	F125W	(26.22 ± 0.19) ^b
6.70905	1498	<i>HST</i> +WFC3	F160W	25.08 ± 0.07
9.29904	1498	<i>HST</i> +WFC3	F160W	25.83 ± 0.14
13.96139	1498	<i>HST</i> +WFC3	F160W	27.10 ± 0.44
178.56572	1498	<i>HST</i> +WFC3	F160W	(25.67 ± 0.13) ^b

Notes.

^a These values have not been corrected for the Galactic extinction of $A_V = 0.06$ mag (Schlafly & Finkbeiner 2011).

^b Quote to the underlying source S1, which lies at about 0.2 s southeast.

$\nu^{-0.75}$, then fitting⁵ the GROND and *HST* data with a broken power-law decay, we find a break at $t = 3.73 \pm 0.16$ days, and the decay indices are 1.49 ± 0.04 and 2.61 ± 0.12 , respectively. This fit yields a total $\chi^2/\text{dof} = 27.8/22$, indicating a reasonable fit for both spectral and temporal behavior of the afterglow. Note that the pre-break decline behavior is also well consistent with the theoretical model (for $p = 2.5$, it is $(3p - 2)/4 \sim 1.4$). The *Swift* XRT PC mode spectrum, although taken earlier than *HST* observations, gives a photon index of $2.00^{+0.19}_{-0.18}$ (Melandri et al. 2015), which is consistent with $p \sim 2.5$, supposing the X-ray band is above both ν_m and ν_c (i.e., the spectrum should be $\propto \nu^{-p/2}$). The data strongly prefer a broken power-law model to a single power-law model, by which the fit gives a $\chi^2/\text{dof} = 97.5/24$. Knust et al. (2017) identified an optical plateau lasting about ~ 8 hr and attributed such a shallow decline to the energy injection from a central millisecond magnetar. This is not at odds with our jet-break interpretation because at late times (i.e., when the magnetar spined down and the energy injection rate drops with time as t^{-2}) the energy injection was not efficient any longer and the forward shock emission

⁵ Here and after, we have fitted the data by the minimal χ^2 method, using the MINUIT package (<http://lcfapp.cern.ch/project/csl/work-packages/mathlibs/minuit/index.html>), and the errors are derived by the MINUIT. The χ^2 is calculated as $\sum \left(\frac{\text{measured value} - \text{predicted value}}{\text{measured error}} \right)^2$, where the *predicted value* is the average flux/magnitude of the predicted light curve within each time bin.

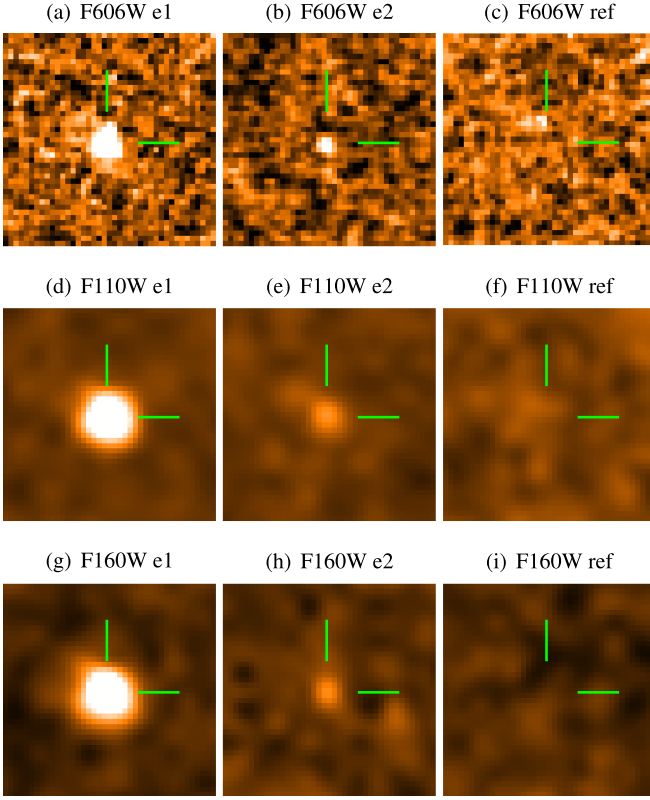


Figure 3. *HST* observations of GRB 160821B. The afterglow emission were detected in all bands in the first two epochs of observations, and faded away in later epochs. In the images of the last epoch, which we take as references, no source is reliably detected near the afterglow position.

Table 2
Observations of GRB 160821B

Time ^a (days)	Exposure (s)	Instrument	Filter	Magnitude ^b (AB)
3.64375	2484	<i>HST</i> +WFC3	<i>F606W</i>	26.00 ± 0.04
10.39618	2484	<i>HST</i> +WFC3	<i>F606W</i>	28.0 ± 0.3
23.16018	1350	<i>HST</i> +WFC3	<i>F606W</i>	$>27.9^b$
103.40406	2484	<i>HST</i> +WFC3	<i>F606W</i>	\dots^c
3.77481	2397	<i>HST</i> +WFC3	<i>F110W</i>	24.78 ± 0.03
10.52723	2397	<i>HST</i> +WFC3	<i>F110W</i>	26.7 ± 0.2
23.18086	1498	<i>HST</i> +WFC3	<i>F110W</i>	$>28.0^b$
99.26591	5395	<i>HST</i> +WFC3	<i>F110W</i>	\dots^c
3.70861	2397	<i>HST</i> +WFC3	<i>F160W</i>	24.50 ± 0.04
10.46105	2397	<i>HST</i> +WFC3	<i>F160W</i>	26.9 ± 0.3
23.23040	2098	<i>HST</i> +WFC3	<i>F160W</i>	>27.0

Notes.

^a These values have not been corrected for the Galactic extinction of $A_V = 0.04$ mag (Schlafly & Finkbeiner 2011).

^b Images have been combined with later exposures as references.

^c Images have been combined to earlier exposures as references.

should be rather similar to the normal scenario (i.e., without energy injection; as shown for example in Zhang et al. 2004).

For GRB 160821B, the publicly available data are rather limited. The *HST* took two epochs of observations at 3.6 days and 10.4 days after the burst, when the afterglow was still visible. Fitting *F606W*, *F110W*, and *F160W* bands with a same power-law decay yields a flux decline $\propto t^{-1.83 \pm 0.13}$ ($\chi^2/\text{d.o.f} = 1.65/2$) (see Figure 6). Fitting the *F606W*, *F110W*, and *F160W* band SED with a power-law spectrum, we find the power-law

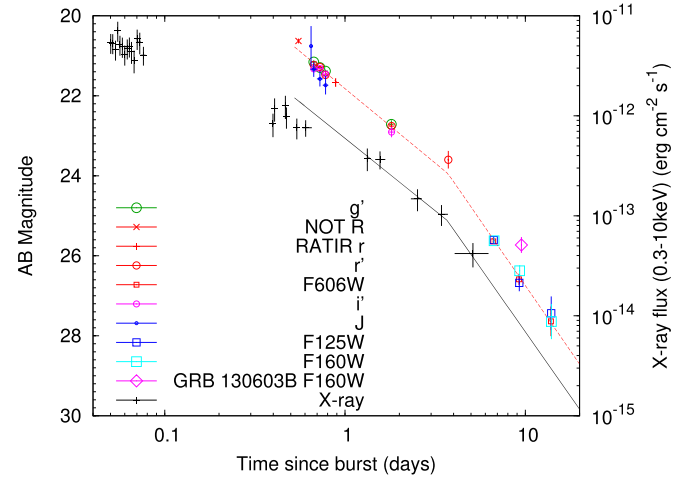


Figure 4. Multi-band afterglow light curves of GRB 150424A. The g' , r' , i' , and J band data are taken from Knust et al. (2017); for the *HST* data analyzed in this work, all bands have been converted to i' band assuming a $\beta = 0.75$ power-law spectrum (note that the *Swift* UVOT and GROND spectra are similar to the *HST* spectrum, as shown in Figure 5). Dashed line is a broken power-law fit to the light curve. Our fit does not include the NOT R band (Malesani et al. 2015) and RATIR r band (Butler et al. 2015) data from GCN. The *Swift* XRT light curve is provided by the UK *Swift* Science Data Centre (Evans et al. 2009), the black line is extrapolated from i' band also with a $\propto \nu^{-0.75}$ spectrum; it is also in agreement with the data.

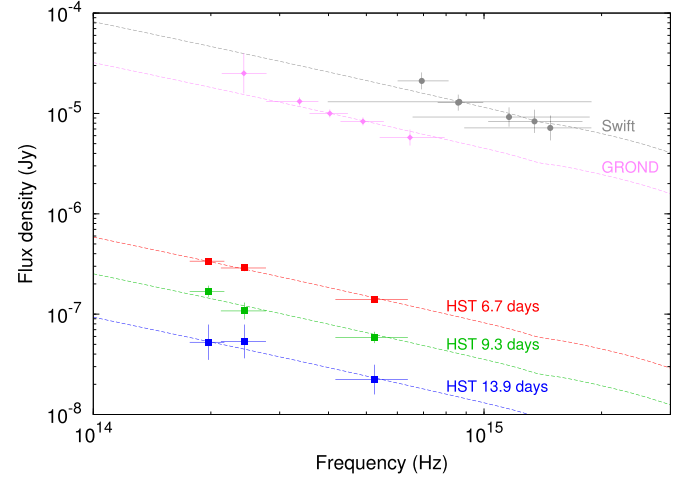


Figure 5. Optical SED of the afterglow of GRB 150424A. The *HST* data are analyzed in this work, and they are fitted by a power-law spectrum with extinction of the Galaxy $E(B - V) = 0.06$ (Schlafly & Finkbeiner 2011). Extinction of the host galaxy is not considered here because there is no significant evidence for such an effect. The *Swift* UVOT data (*uvw2*, *uvm2*, *uvw1*, *white*, *u* and *b* bands) are adopted from Marshall & Beardmore (2015), the GROND data (g' , r' , i' , z' , and J bands) are taken from Kann et al. (2015), and their power-law spectra are similar to the *HST*'s. Note that the UVOT data were not measured simultaneously. However, the afterglow emission changed very slowly at early times, as shown in Knust et al. (2017). Moreover, the UVOT data reported in Marshall & Beardmore (2015) are combinations of images during similar time intervals. It is thus reasonable to use these UVOT data to construct a SED.

indices are $\alpha = 1.35 \pm 0.07$ ($\chi^2/\text{d.o.f} = 13/1$) at $t = 3.6$ days and $\alpha = 1.12 \pm 0.39$ ($\chi^2/\text{d.o.f} = 3.36/1$) at $t = 10.4$ days, respectively. Alternatively, if we fit the data with a thermal spectrum, the resulting temperature is of $4488 \pm 81[(1+z)/1.16]$ K ($\chi^2/\text{d.o.f} = 15/1$) at $t = 3.6$ days and $= 4750 \pm 473 [(1+z)/1.16]$ K ($\chi^2/\text{d.o.f} = 0.30/1$) at $t = 10.4$ days, respectively. Though a thermal spectrum can well reproduce the SED at $t = 10.4$ days, the temperature is much higher than ~ 2500 K,

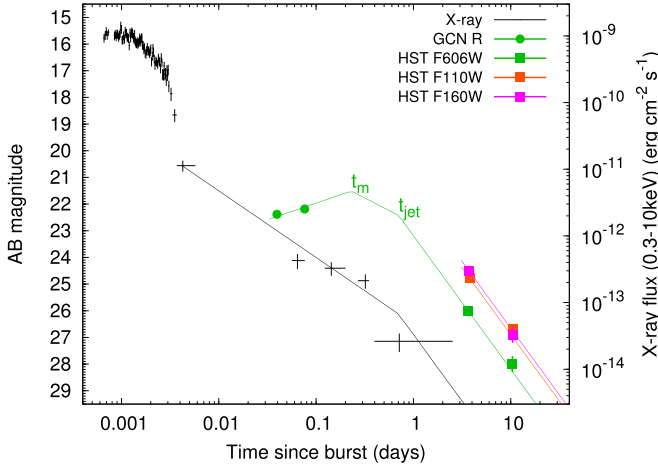


Figure 6. Multi-band afterglow light curves of GRB 160821B. *HST* data can be fitted by a power-law decay with index 1.83 ± 0.13 ($\chi^2/\text{d.o.f} = 1.65/(6-4)$). The *R* band data are from NOT (Xu et al. 2016) and GTC (Jeong et al. 2016), the *Swift* XRT light curve is provided by the UK *Swift* Science Data Centre (Evans et al. 2009). Though rather sparse, they can be interpreted by a simple analytic afterglow model (green and black lines). The forward shock emission was in the slow cooling phase and the spectral index of the accelerated electrons (p) is about 2. For $t < t_m$, the *R* band is below ν_m and the flux increases with the time as $t^{1/2}$. At $t = t_m$, ν_m crossed the *R*-band, then the flux drops with the times as $t^{-(p-1)/4}$. At $t > t_{\text{jet}}$, the flux declines as t^{-p} (the spectra at $t \geq 3.6$ days, however, suggest that at late times the optical bands are below both ν_m and ν_c). As for the X-ray emission, the observer’s frequency is above both ν_m and ν_c , and the decline is $\propto t^{-(3p-2)/4}$ for $t < t_{\text{jet}}$ and $\propto t^{-p}$ for $t > t_{\text{jet}}$.

the value inferred for the macronova signals of GRB 060614 and GW170817/GRB 170817A in a similar epoch (see Jin et al. 2015; Drout et al. 2017, respectively). Instead, the overall decline behavior as well as the power-law spectrum at $t = 10.4$ days are largely consistent with the jet model for $p \sim 2$ and $\nu_{\text{obs}} > \max\{\nu_m, \nu_c\}$ (the spectrum is $\propto \nu^{-p/2}$). Moreover, the *Swift* XRT spectrum measured in the time interval of $t \sim 4873\text{--}47180$ s has a power-law photon index $2.0^{+0.7}_{-0.6}$ (<http://www.swift.ac.uk/xrt-spectra/00709357/>; Evans et al. 2009), which is consistent with $p \sim 2$, too. Supposing the sideways expansion of the ejecta is unimportant, at early times the flux declines as $t^{(2-3p)/4}$ while in the post-jet-break phase the decline is steepened by a factor of $t^{-3/4}$, as shown in Zhang & Mészáros (2004). Therefore, we suggest that the *HST* data of GRB 160821B were dominated by a power-law afterglow component though at $t = 3.6$ days an underlying weak macronova component is possible (please see Section 2.3 for further discussion). The X-ray afterglow emission in the time interval of $\sim 0.05\text{--}2$ day after the burst also strongly indicate the presence of a jet break at $t \geq 0.3$ day. The analytical approach yields a $t_{\text{jet}} \sim 0.7$ day (see Figure 6), which is comparable to though a bit larger than the X-ray data based estimate by Lü et al. (2017).

With the break time, the jet half-opening angle can be estimated by (Sari et al. 1999; Frail et al. 2001)

$$\theta_j \approx 0.076 \left(\frac{t_{\text{jet}}}{1 \text{ day}} \right)^{3/8} \left(\frac{1+z}{2} \right)^{-3/8} \left(\frac{E_{\text{iso}}}{10^{51} \text{ erg}} \right)^{-1/8} \times \left(\frac{\eta_\gamma}{0.2} \right)^{1/8} \left(\frac{n}{0.01 \text{ cm}^{-3}} \right)^{1/8}. \quad (1)$$

For GRB 150424A, Konus-Wind recorded a total gamma-ray (20 keV–10 MeV) fluence of $1.81 \pm 0.11 \times 10^{-5} \text{ erg cm}^{-2}$

Table 3
Short/lsGRBs with a Jet Break (or Upper Limit)

GRB	z	E_{iso} (10^{51} erg)	t_{jet} (days)	θ_j (rad)	References
050709	0.16	0.07	< 1.4	< 0.14	(1)
051221A	0.546	2.4	5	0.09	(2), (3)
060614	0.125	2.5	1.4	0.08–0.09	(4), (5)
061201	0.111	0.14	0.03	0.02–0.03	(6)
090426A	2.609	4.2	0.4	0.08–0.12	(7)
111020A	...	$0.21/1.9^a$	2	0.05–0.14	(8)
130603B	0.356	2.1	0.47	0.07–0.14	(9), (10)
140903A	0.351	0.06	1.2	0.05–0.1	(11), (12)
150424A	0.30	4.3	3.7	0.12	this work
160821B	0.16	0.21	0.7	0.10	this work, (13)

Notes.

^a The isotropic-equivalent prompt emission energy was roughly estimated in Equation (8) by assuming different redshifts and physical parameters.

References. (1) Jin et al. (2016), (2) Soderberg et al. (2006), (3) Burrows et al. (2006), (4) Xu et al. (2009), (5) Mangano et al. (2007), (6) Stratta et al. (2007), (7) Nicuesa Guelbenzu et al. (2011), (8) Fong et al. (2012), (9) Fong et al. (2014), (10) Fan et al. (2013), (11) Troja et al. (2016a), (12) Zhang et al. (2017), (13) Lü et al. (2017).

(Golenetskii et al. 2015), corresponding to an isotropic gamma-ray emission energy of $E_{\text{iso}} \sim 4.3 \times 10^{51}$ or $\sim 1.0 \times 10^{53}$ erg at $z = 0.3$ or 1.0 , respectively, using cosmological parameters of Planck results (Planck Collaboration et al. 2014). The Fermi gamma-ray (10–1000 keV) fluence is $1.68 \pm 0.19 \times 10^{-6} \text{ erg cm}^{-2}$ for GRB 160821B (Stanbro & Meegan 2016), so we have $E_{\text{iso}} \sim 10^{50}$ erg for $z = 0.16$. Following Frail et al. (2001) we take the radiation efficiency $\eta_\gamma = 0.2$. For the ISM number density $n = 0.01 \text{ cm}^{-3}$ (see Fong et al. 2015 for the evidence of the low number density of the ISM surrounding SGRBs), we get $\theta_j \approx 0.12$ for GRB 150424A (if we take $z = 1.0$ then $\theta_j \sim 0.07$) and $\theta_j \approx 0.1$ for GRB 160821B.

A reliable jet half-opening angle has only been rarely inferred for SGRBs/lsGRBs (Please see Table 3 for a summary). Interestingly, all low-redshift ($z \leq 0.4$) events (except GRB 050502B, of which the optical afterglow emission was never detected) with deep *HST* follow-up observations are in this sample. These events include GRB 050709, GRB 060614, GRB 130603B, GRB 150424A, and GRB 160821B (note that for GRB 050709, no jet break was directly measured. But the presence of a macronova signal strongly favors a jet break at $t \leq 1.4$ days after the burst; see Jin et al. 2016). Such an observational fact likely points toward the presence of jet break in most events and their non-detection may simply due to the lack of deep follow-up observations. The other interesting feature is the “narrow” distribution of these estimated θ_j that peaks at ~ 0.1 rad, indicating that many more SGRBs/lsGRBs were off-beam (or off-axis).

2.3. Any Macronova Signal in GRB 150424A and/or GRB 160821B?

For GRB 150424A, both the temporal and spectral behaviors are well consistent with the afterglow model and there is no macronova signal; see Figures 4 and 5.

As for GRB 160821B, the situation is less clear. The *HST* data at $t \sim 3.6$ days are hard to be interpreted as either a power-law or a thermal spectrum (see Section 2.2). Interestingly, they can be interpreted as the superposition of a power-law afterglow component (with a spectrum $f_\nu \propto \nu^{-1.1}$) and a thermal-like

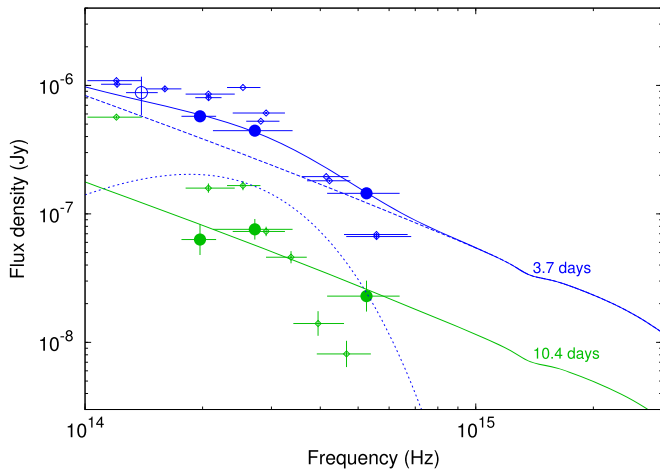


Figure 7. SED of GRB 160821B. Big solid circles represent *HST* F606W, F110W, and F160W band data measured at 3.6 days and 10.4 days after the burst, and the single big empty circle is the Keck K_s band data measured at 4.3 days (Kasliwal et al. 2017a). As the spectrum at $t \sim 3.6$ days cannot be reasonably fitted by a single power, here we fit the data by a power-law component (dashed lines) plus a weak thermal (dotted lines) component. Due to the rarity of the data, the power-law index and the temperature are fixed to 1.1 and 3100 K. The Galactic extinction of $E(B - V) = 0.04$ mag (Schlafly & Finkbeiner 2011) has been taken into account in the fit, while the extinction of the host galaxy is not considered because of the lack of relevant data. The SED has also been compared with AT2017gfo, the macronova associated with the gravitation wave event GW170817, which has been shifted from $z = 0.0095$ to $z = 0.16$. The data of AT2017gfo (in diamond) are from VLT (Pian et al. 2017), Gemini (Kasliwal et al. 2017b; Troja et al. 2017) and VISTA (Tanvir et al. 2017), and corrected for the Galactic extinction of $E(B - V) = 0.11$ (Schlafly & Finkbeiner 2011). Although the afterglow flux of GRB 160821B in F110W and F160W bands are comparable with AT2017gfo (shifted to $z = 0.16$), their SEDs are, however, quite different (i.e., the latter is much softer). Thus, we suggest that the afterglow of GRB 160821B is dominated by a power-law spectrum component, but a weak underlying macronova component with a flux of $\sim 1/5$ that of AT2017gfo is possible.

component with a temperature of ~ 3100 K (due to the sparse data points, this temperature is fixed to be that of AT2017gfo in the same epoch⁶) and the fit yields $\chi^2/\text{d.o.f} = 1.36/1$, as shown in Figure 7. Such a result is likely to support the speculation of Troja et al. (2016b) that there might be a weak macronova signal in the afterglow of GRB 160821B. Though intriguing, the current limited publicly available *HST* data alone are insufficient to draw a final conclusion (T. Piran 2017, private communication).

2.4. The Neutron Star Merger Rate in the Local ($z \leq 0.2$) Universe

The SGRB data-based neutron star merger rate was widely estimated in the literature (e.g., Guetta & Piran 2005; Nakar 2007; Coward et al. 2012; Fong & Berger 2013; Petrillo et al. 2013; Fong et al. 2015). However, all these previous approaches were mainly based on jet opening angles measured at relatively high redshifts (though GRB 050709, GRB 060614, and GRB 061201 were included “individually” in some estimates). The reasonable estimate of θ_j for GRB 050709, GRB 060614, GRB 061201, and GRB 160821B, four GRBs at

redshifts of ≤ 0.2 , provides the first opportunity to directly though conservatively estimate the neutron star merger rate in the local universe that can be directly tested by (compared with) the ongoing advanced LIGO/Virgo observations.

GRB 050709 was detected by *HETE-II* with a field of view (FoV) ≈ 3 sr (Villasenor et al. 2005), while GRB 060614, GRB 061201, and GRB 160821B were recorded by the *Swift* satellite with a FoV ≈ 1.4 – 2.4 sr (Gehrels et al. 2006; Siegel et al. 2016). Note that *HETE-II* has a much lower detection rate of SGRBs in comparison with *Swift* due to the relatively small effective area of the on board detector. Moreover, no GRBs were reported by *HETE-II* any longer since 2006 March (<http://space.mit.edu/HETE/Bursts/>). The joint analysis of *HETE-II* and *Swift* SGRBs are thus very challenging. In this work, for simplicity we exclude GRB 050709 in the following investigation.

Now we evaluate the “apparent” (i.e., without the jet half-opening angle correction) rate, $\mathcal{R}_{\text{nsm,app}}$, for local SGRBs. The apparent rate is related to the observational number of events as well as the sensitivity and FoV of the instrument. For a given redshift, the sensitivity plays a role in determining the weakest SGRB that can be detected by the instrument while the F.o.V reflects the search portion of the full sky. The BAT on board *Swift* is a coded mask telescope, and its F.o.V and sensitivity change as a function of the partial coding fraction, which is related to the burst’s incident angle (Barthelmy et al. 2005); meanwhile, BAT has a complex trigger algorithm, making detailed analysis on the intrinsic rate through *Swift* data very complicated (Lien et al. 2014). In this work, we take into account these effects as the following: Lien et al. (2016) showed that the sensitivity of BAT decreases with the burst’s duration (which roughly reflects the exposure time) with $\text{flux}_{\text{limit}} \propto 1/\sqrt{T_{90}}$; they also showed that the sensitivity to 1s flux is $\sim 3 \times 10^{-8} \text{ erg cm}^{-2} \text{ s}^{-1}$ for fully coded region. If a burst’s incident angle is large, and the detector’s plane is partially coded, the effect of partial coding fraction p_f can be expressed with the “effective on-axis exposure time” $T_{\text{eff}} = p_f T_{90}$ (Baumgartner et al. 2013). With these relations, we collect the 1s peak fluxes of the three bursts from the *Swift*/BAT Gamma-Ray Burst Catalog and calculate the corresponding smallest partial coding at different distances by

$$p_f = \left[\frac{3 \times 10^{-8} \text{ erg/cm}^2/\text{s}}{\left(\frac{D_{L0}}{D_L}\right)^2 \left(\frac{1+z}{1+z_0}\right) f_0} \right]^2 / T_{90}, \quad (2)$$

where z_0 , D_{L0} , and f_0 are the observed redshift, luminosity distance, and 1s peak flux, respectively, of a given burst. The yielded p_f is then used to calculate the corresponding BAT FoV, and their relation are inferred from Barthelmy et al. (2005) (we fit their simulated curve adjusted for off-axis projection effects with polynome and obtain a analytical function $\text{F.o.V}(p_f)$). The FoV is then adopted to calculate the spacetime volume of the search for a given burst:

$$\langle VT \rangle = 0.9T \int_0^{0.2} \frac{\text{F.o.V}(p_f)}{4\pi} \frac{1}{1+z} \frac{dV_c(z)}{dz} dz, \quad (3)$$

where the factor 0.9 represents the fraction of the time that BAT spends on searching for GRBs. Assuming a negligible evolution of rate in the local universe, and the observed number of event in a given spacetime volume should follow a Poission distribution, we use the Bayesian inference to derive the

⁶ One can also assume that at $t = 10.4$ days, there is also a thermal component at a temperature of ~ 2500 K. A $f_\nu \propto \nu^{-1.1}$ power-law spectrum plus such a thermal component fit finds out that the thermal component has a flux lower than the data points by a factor of ~ 10 . Indeed, as revealed in AT2017gfo, the late time optical/infrared macronova emission (e.g., Kasliwal et al. 2017b; Pian et al. 2017; Tanvir et al. 2017) drops with time quicker than t^{-3} .

posterior distribution of $\mathcal{R}_{\text{nsm,app}}$ for each burst by (see Wang et al. 2017, and references therein)

$$P(\mathcal{R}_{\text{nsm,app}}) \propto P_{\text{Poisson}}(1|\Lambda) \times P'(\mathcal{R}_{\text{nsm,app}}), \quad (4)$$

where $P_{\text{Poisson}}(1|\Lambda)$ is the likelihood of observing one event from a Poisson distribution with a mean number $\Lambda = \mathcal{R}_{\text{nsm,app}} \langle VT \rangle$, and $P'(\mathcal{R}_{\text{nsm,app}})$ is the prior (for which we choose a uniform distribution). The inferred rates from GRB 060614, GRB 061201 and GRB 160821B are $0.25^{+0.37}_{-0.18}$, $0.26^{+0.40}_{-0.19}$ and $0.30^{+0.45}_{-0.22} \text{ Gpc}^{-3} \text{ yr}^{-1}$, respectively. In this work, the errors stand for the 68% credible intervals unless specifically noted. These rates are similar, indicating that these three bursts are bright and hence the influence from the change of F.o.V is not significant.

To get the local neutron star merger rate, the geometry correction (including the uncertainties of θ_j) should be addressed. We assume that the probability distribution of the true values of θ_j of GRB 060614 and GRB 061201 follow uniform distribution in the intervals reported in Table 3. For GRB 160821B, we assume its θ_j distributes uniformly within 0.08–0.18 rad since t_{jet} should be within ~ 0.3 –3 days after the burst (see the X-ray and optical data in Figure 6). The posterior distribution of local neutron star merger rate derived from each burst, \mathcal{R}_{nsm} , is then calculated by

$$p(\mathcal{R}_{\text{nsm}}) \propto \int_{\theta_{j,\min}}^{\theta_{j,\max}} p(1|\mathcal{R}_{\text{nsm}}, \theta_j) p'(\mathcal{R}_{\text{nsm}}) p'(\theta_j) d\theta_j \quad (5)$$

in which the priors for θ_j follow the distributions discussed above, and the prior for \mathcal{R}_{nsm} is assume to be uniform. The likelihood term can be written as

$$p(1|\mathcal{R}_{\text{nsm}}, \theta_j) = p_{\text{poisson}} \left(1 | \mathcal{R}_{\text{nsm}} \frac{\theta_j^2}{2} \langle VT \rangle \right). \quad (6)$$

The local neutron star merger rates inferred from GRB 060614, GRB 061201, and GRB 160821B are 68^{+103}_{-50} , 832^{+1407}_{-625} and $33^{+84}_{-27} \text{ Gpc}^{-3} \text{ yr}^{-1}$, respectively. The total rate, dominated by GRB 061201, is obtained by convoluting the three distributions together, with which we have

$$\mathcal{R}_{\text{nsm}} = 1109^{+1432}_{-657} \text{ Gpc}^{-3} \text{ yr}^{-1}. \quad (7)$$

Correspondingly, the total rate with the 90% credible interval is $1109^{+2872}_{-840} \text{ Gpc}^{-3} \text{ yr}^{-1}$.

Besides the issues examined above, some other factors may further increase the uncertainties to our results (see e.g., Coward et al. 2012). (a) The redshift of GRB 061201 is less secure (Stratta et al. 2007) than the other events.⁷ Because our sample number is small, this will increase the uncertainty of the result. In the following, we will exclude GRB 061201 and do the calculation again for comparison. (b) Only $\lesssim 1/4$ of the SGRBs have measured redshifts (Berger 2014) and some other SGRBs could be nearby, too.⁸ For example, recently Siellez et al. (2016) claimed

⁷ Note that for $z = 0.111$, the inferred $\theta_j \lesssim 2$ deg is already a few times smaller than the others reported in Table 3. At a redshift ~ 1 , one has $\theta_j \lesssim 0.5$ deg (Stratta et al. 2007), which is hard to understand in the short GRB scenario. Such a fact likely disfavors the high-redshift hypothesis, which is why in this work we take the \mathcal{R}_{nsm} reported in Equation (7) as the fiducial value though the exclusion of GRB 061201 will yield a significantly lower merger rate.

⁸ For the local merger-driven GRBs, the situation will change dramatically in the GW era since the gravitational wave data alone can yield reliable luminosity distance and hence the missing z problem will be solved. The intense deep follow-up observations of the GW/GRB events are also extremely helpful in measuring the jet breaks of the afterglows.

that GRB 070923 and 090417A were at $z < 0.1$. Moreover, in our analysis two “local” bursts (GRB 080905A and GRB 150101B) without a reliable jet opening angles are excluded in the rate estimate. It is also probable that only a fraction of neutron star mergers can produce either SGRBs or lsGRBs. Taking into account these factors, the real neutron star merger rate density should be enhanced by a factor of $f_c > 1$. As a conservative estimate on \mathcal{R}_{nsm} , we do not correct this further. (c) There are arguments that GRBs shorter than 2 s may have collapsar origin, while bursts with duration longer than 2 s may still have non-collapsars origin (Bromberg et al. 2013). This is indeed the case for GRB 060614, which is a long-duration burst, but the identified macronova component in its late afterglow (Jin et al. 2015; Yang et al. 2015) revealed its neutron star merger origin. For the other nearby events (GRB 050709, GRB 061201, and GRB 160821B), no supernova emission were detected down to very stringent limits, which strongly disfavored the collapsar origin. Therefore, for our sample, this correction is likely irrelevant. (d) Due to its limited energy range, the SGRB detection rate of *Swift* is found to be a factor of $R_{\text{b/s}} = 6.7$ lower than that of BATSE. Coward et al. (2012) amplified the *Swift* SGRB rate by such a factor to crudely correct the bias. Though interesting, it is unclear whether this is a reasonable approximation for the local events that are of our interest. Moreover, such a correction likely enhances the merger rate. In summary, despite all these factors playing roles in the rate estimation, only point (a) seems to be able to significantly change our “conservative” estimate. If we exclude GRB 061201 from the sample, the apparent SGRB rate and neutron star merger rate are $0.81^{+0.60}_{-0.39} \text{ Gpc}^{-3} \text{ yr}^{-1}$ and

$$\mathcal{R}_{\text{nsm,w/o 061201}} = 162^{+140}_{-83} \text{ Gpc}^{-3} \text{ yr}^{-1}, \quad (8)$$

respectively. The resulting neutron merger rate is significantly smaller than that found in Equation (7), suggesting that our results are sensitively dependent on the narrowly beamed burst GRB 061201, and a larger sample is crucial to get a more reliable estimate on \mathcal{R}_{nsm} .

Intriguingly, the successful detection of GW170817 in the O2 run of advanced LIGO yields a neutron star merger rate of (Abbott et al. 2017)

$$\mathcal{R}_{\text{nsm,gw}} = 1540^{+3200}_{-1220} \text{ Gpc}^{-3} \text{ yr}^{-1},$$

which is in agreement with the local SGRB-based neutron star merger rate reported in Equation (7). For Equation (8), the consistence with $\mathcal{R}_{\text{nsm,gw}}$ is marginal.

The advanced LIGO detectors can detect the gravitational wave radiation from double neutron star mergers within a typical distance $D \sim 220$ Mpc at its designed sensitivity (Abadie et al. 2010). The detection rate of neutron star mergers is thus

$$R_{\text{gw,nsm}} = \frac{4\pi D^3}{3} \mathcal{R}_{\text{nsm,gw}} \sim 69^{+143}_{-55} \text{ yr}^{-1} \left(\frac{D}{220 \text{ Mpc}} \right)^3. \quad (9)$$

Notice that the above number assumes a perfect GW detector; a realistic one operates with a duty cycle and in reality the expected value would decrease by the coincident duty cycle. Nevertheless, the detection prospect is indeed quite promising and we expect that much more binary neutron star merger events will be detected in the near future.

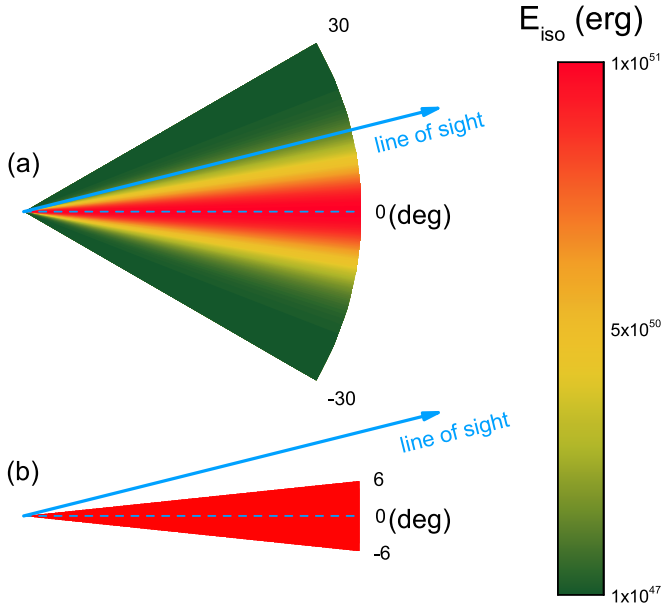


Figure 8. (a) Illustration of the off-axis scenario in the structured jet model. (b) Illustration of the off-beam scenario in the uniform jet model.

3. GRB/GW Association: The Contribution of off-beam and off-axis Events

The energy distribution of the GRB ejecta is still unclear. In the standard fireball afterglow model, a conical jet with a uniform energy distribution within the cone and sharp energy depletion at the jet edge are assumed (i.e., $\epsilon(\theta) = \epsilon_0$ for $\theta \leq \theta_j$ otherwise equals to 0, where $\epsilon(\theta)$ denotes the energy distribution of the ejecta as a function of the polar angle θ). To account for the diverse prompt/afterglow emission of LGRBs, it is further proposed that a non-uniform distribution of energy per solid angle within the jet (i.e., the jets are structured) and the widely discussed scenarios include (a) the power-law distribution model $\epsilon(\theta) = \epsilon_0 \theta^{-2}$ for $\theta > \theta_c$ (Dai & Gou 2001; Rossi et al. 2002; Zhang & Mészáros 2002) otherwise $\epsilon(\theta) = \epsilon_0$; (b) the Gaussian-type jet $\epsilon(\theta) = \epsilon_0 \exp(-\theta^2/2\theta_c^2)$ (Zhang et al. 2004), which is illustrated in Figure 8 for $\theta_c \sim 7$ deg and $\epsilon_0 = 10^{51}$ erg; (c) the two-component jet model (Berger et al. 2003; Wu et al. 2005; Huang et al. 2006). The SGRB outflows are likely structured, too, as found in the numerical simulations (Aloy et al. 2005; Murguía-Berthier et al. 2017) and in the afterglow modeling (Jin et al. 2007).

A bright SGRB has a typical isotropic-equivalent kinetic energy of $E_{\text{iso}} \sim 10^{51}$ erg (Zhang et al. 2012; Fong et al. 2015). Such energetic outbursts are detectable for *Swift*, Fermi-GBM and GECam detectors⁹ at a distance of $D \leq 200$ Mpc even when our line of sight is “slightly” outside of the ejecta (note that in this paragraph we adopt the *uniform jet model*). It is known the on-beam and off-beam isotropic energies are different by a factor of $\sim (1 + (\eta\Delta\theta)^2)^3$ (for $\Delta\theta \geq \theta_j$; see

e.g., Rybicki & Lightman 1979), where η is the initial Lorentz factor of the GRB outflow and the viewing angle $\theta_v = \theta_j + \Delta\theta$. Hence we have

$$\Delta\theta \leq 0.04 \left[\frac{E_{\text{iso}}}{10^{51} \text{ erg}} \right]^{1/6} \left(\frac{\eta}{100} \right)^{-1} \left(\frac{D}{200 \text{ Mpc}} \right)^{-1/3} \times \left(\frac{\mathcal{F}_{\text{th}}}{10^{-7} \text{ erg cm}^{-2}} \right)^{-1/6}, \quad (10)$$

where $\mathcal{F}_{\text{th}} \sim 10^{-7} \text{ erg cm}^{-2}$ is the fluence threshold for a reliable detection of a weak GRB by Fermi-GBM like detector. The η has been normalized to ~ 100 , motivated by the Lorentz factor–luminosity correlation of GRBs (Liang et al. 2010; Fan et al. 2012; Lü et al. 2012). Unless $\eta \leq 50$, we have $\Delta\theta < \theta_j (\sim 0.1)$, implying that in the uniform jet model, the off-beam events can enhance the GRB/GW association at most moderately (the enhancement factor is estimated as $\mathcal{R} \approx (\theta_j + \Delta\theta)^2/\theta_j^2$). Such events should be observed mainly in X-rays and last longer, since the energy of the gamma-rays is lowered by a factor of $a_0 = [1 + (\eta\Delta\theta)^2]^{-1}$ and the duration is extended by a factor of a_0^{-1} .

In the *structured jet model*, GRB/GW associations are more common. In the numerical simulations, relativistic outflows with $\eta \geq 10$ and $\epsilon(\theta \leq \theta_{\text{cut}}) \geq 10^{48} \text{ erg}$ are found within the polar angle of $\theta_{\text{cut}} \lesssim 0.3\text{--}0.4$ rad (Aloy et al. 2005; Gottlieb et al. 2017; Murguía-Berthier et al. 2017). The photospheric radius of a relativistic outflow reads $R_{\text{ph}} \approx 4 \times 10^{11} \text{ cm} (L_{\text{tot}}/10^{48} \text{ erg s}^{-1})(\eta/10)^{-3}$, where L_{tot} is the total luminosity of the outflow (Paczynski 1990). The initial radius of the “reborn” fireball is $R_0 \sim 10^9 \text{ cm}$ (Aloy et al. 2005). As long as R_{ph} is in the same order of ηR_0 , the thermal radiation will be efficient, requiring that (one can get the following expression with for example Equation (9) of Fan & Wei 2011, by setting $f \sim 1$)

$$\eta \sim 25 (L_{\text{tot}}/10^{48} \text{ erg s}^{-1})^{1/4} (R_0/10^9 \text{ cm})^{-1/4}. \quad (11)$$

The temperature of the emission can be estimated as $T_{\text{obs}} \sim 20 \text{ keV} (L_{\text{tot}}/10^{48} \text{ erg s}^{-1})^{1/4} (R_0/10^9 \text{ cm})^{-1/2} (\eta/25)^{8/3}$. The corresponding peak energy of the observed spectrum (ν_f) is thus

$$E_p \sim 3.92 T_{\text{obs}} \sim 78 \text{ keV} (L_{\text{tot}}/10^{48} \text{ erg s}^{-1})^{1/4} \times (R_0/10^9 \text{ cm})^{-1/2} (\eta/25)^{8/3}, \quad (12)$$

where the redshift correction has been ignored since in this work we concentrate on the nearby events. The emission duration is likely determined by the width of the ejecta in the direction of the line of sight. Such emission, if within a distance of ~ 200 Mpc, are detectable for *Swift*, GECam and Fermi-GBM like detectors since the corresponding flux is $\gtrsim 10^{-7} \text{ erg cm}^{-2} \text{ s}^{-1}$ for a γ -ray luminosity of $\sim 5 \times 10^{47} \text{ erg s}^{-1}$. The association chance between these weak GRB-like transients and GW events is larger than that between the bright SGRBs and GW events by a factor of

$$\mathcal{R} \sim \frac{1 - \cos \theta_{\text{cut}}}{1 - \cos \theta_j} \sim 16 \frac{(\theta_{\text{cut}}/0.4 \text{ rad})^2}{(\theta_j/0.1 \text{ rad})^2}, \quad (13)$$

implying a more promising prospect of establishing the GRB/GW association in the near future. Note that here $\theta_{\text{cut}} \sim 0.4 \text{ rad}$ is adopted to match the structured jet edge found in some numerical simulations. Moreover, a Gaussian-type jet

⁹ Fermi-GBM and GECam like detectors are benefited for their very wide field of view (Meegan et al. 2009; S. L. Xiong et al. 2018, in preparation), which is very important for catching the GRB/GW association events. *Swift* has a sensitivity much higher than Fermi-GBM and comparable to GECam but its field of view is just $\sim 1.4\text{--}2.4$ sr. The proposing GECam mission (S. L. Xiong et al. 2018, in preparation) is designed to cover 90% of the sky at a sensitivity of $2 \times 10^{-8} \text{ erg cm}^{-2} \text{ s}^{-1}$ in the energy range of 8 keV–2 MeV. Its location accuracy is of ~ 1 square degrees. All these properties make GECam a very suitable detector to record the GW-associated GRB signals.

$\epsilon(\theta) \approx 10^{50-51} \text{ erg exp}(-\theta^2/2\theta_c^2)$ will yield $\epsilon(\theta = 0.38 \text{ rad}) \sim 10^{47-48} \text{ erg}$ for $\theta_c \sim 0.1 \text{ rad}$, which is detectable for the GECam detector as long as the events are within a distance of $\sim 200 \text{ Mpc}$ (S. L. Xiong et al. 2018, in preparation). The other prediction of the off-axis ejecta model is an unambiguous re-brightening of the afterglow due to the emergence of the forward shock emission of the energetic ejecta core (Kumar & Granot 2003; Wei & Jin 2003). Recently, Lamb & Kobayashi (2017) calculated such emission and suggested them as one of the most promising electromagnetic counterparts of neutron star mergers that may be able to outshine the macronova/kilonova emission (these authors also mentioned the prompt emission but did not go further). Because the beam-corrected SGRB rate (see Equation (7)) is roughly comparable to the gravitational wave event-based estimate (Abbott et al. 2017), it may be reasonable to speculate that SGRBs were produced in a good fraction of mergers, for which the GRB/GW association probability may be as high as $\sim \theta_{\text{cut}}^2/2 \sim 10\%$. The prospect of establishing the GRB/GW association is thus more promising than that suggested in the literature (Williamson et al. 2014; Clark et al. 2015; Li et al. 2016).

Very recently, Lazzati et al. (2017) calculated the emission from the possible wide cocoon (i.e., within the polar angle $\sim 40^\circ$) surrounding the SGRB outflow and suggested the prompt X-ray emission with $E_{\text{iso}} \sim 10^{49} \text{ erg}$, which is significantly stronger than our signal. Such kind of energetic shortly lasting X-ray outbursts will be nice electromagnetic counterparts of GW events (see, however, Gottlieb et al. 2017 for the results based on the 3D simulation).

In the above discussion, the successful launching of GRB ejecta is assumed. This may be not always the case. As already revealed by the numerical simulations, some relativistic ejecta cannot break out successfully if the initial half-opening angles are too wide (see e.g., Aloy et al. 2005; Nagakura et al. 2014; Murguía-Berthier et al. 2017). In such cases, low-luminosity events may be powered by the mildly relativistic outflow. The simple thermal radiation model, however, is usually unable to give rise to significant emission at energies above 10 keV for $\eta \leq 10$ (not that as long as $R_{\text{ph}} \gg \eta R_0$, we have $E_p \propto \eta^{8/3}$) and additional physical process(es) (e.g., shocks, or magnetic energy dissipation, or shock breakout) should be introduced to generate X-ray/gamma-ray emission.

4. Summary and Discussion

After the discovery of the SGRB afterglow, dedicated efforts have been made to identify the jet breaks and then infer the half-opening angles. However, the sample increases rather slowly due to the dim nature of these events. The main reason for the non-detection/identification of the jet breaks in most SGRB afterglows may be the lack of deep follow-up observations. The realization that the macronovae may appear within one to two weeks after the GRBs inspired the very late afterglow observations. With these high-quality optical/near-infrared data, we found two jet breaks in GRB 150424A and GRB 160821B. Together with the previous results, we have a SGRB/jet sample consisting of 10 events (including one long-short event). The inferred half-opening angles have a very narrow distribution (i.e., $\theta_j \sim 0.1$). Though the sample is still small, there are four events taking place locally (i.e., $z \leq 0.2$), with which the “local” neutron

star merger rate density has been estimated to be $\sim 1109 \text{ Gpc}^{-3} \text{ yr}^{-1}$ or $\sim 162 \text{ Gpc}^{-3} \text{ yr}^{-1}$ if the narrowly collimated GRB 061201 is excluded. These SGRB-based local neutron star merger rates, however, are conservative because a few “local” SGRBs (including GRB 080905A and GRB 150101B) have not been taken into account; moreover, just $\sim 1/4$ SGRBs have redshifts. Further enhancement is plausible if the SGRB production fraction of neutron star mergers is lower than 100% and the SGRB detection rate by *Swift* seems to be lower than BATSE-like detectors. Nevertheless, more local SGRBs with reasonably measured θ_j are needed to get more reliable \mathcal{R}_{nsm} since the current estimate is seriously affected by the narrowly beamed event GRB 061201.

We have also examined the *HST* data of GRB 150424A and GRB 160821B to search for possible macronova signal(s). In GRB 150424A, no sign has been found. While in GRB 160821B, the *HST* and Keck (Kasliwal et al. 2017a) data at $t \sim 3.6\text{--}4.3 \text{ days}$ can be interpreted as a power-law afterglow component plus a thermal component with a temperature of $\sim 3100 \text{ K}$. However, with the rather limited currently (publicly) available data, no evidence as strong as that for GRB 130603B, GRB 060614, GRB 050709, and GRB 170817A can be provided.


Finally, motivated by the plausible promising detection prospect of neutron star mergers in the near future, we have re-estimated the GRB/GW association probability. For the very nearby (i.e., $D \leq 200 \text{ Mpc}$) events, some off-beam GRBs (in the uniform jet model) may be detectable, possibly appearing as the low-luminosity X-rich transients/GRBs (if the duration of the intrinsic (on-beam) event is dominated by one single pulse, the observed duration would be extended by a factor of $1 + (\eta\Delta\theta)^2$). The enhancement of the GRB/GW association is, however, at most moderate. The situation is different if the merger-driven relativistic ejecta are structured in a wide solid angle. In such a case, the prompt emission of the relativistic ejecta, though viewed off-axis, are detectable for *Swift*, Fermi-GBM and GECam like detectors if the sources are at $D \leq 200 \text{ Mpc}$ and the corresponding GRB/GW association probability may be high up to $\sim 10\%$.

We thank the anonymous referee for helpful suggestions and T. Piran, R. F. Shen, and Y. M. Hu for discussions. This work was supported in part by 973 Programme of China (No. 2014CB845800), by NSFC under grants 11525313 (the National Natural Fund for Distinguished Young Scholars), 11433009, and 11773078, by the Chinese Academy of Sciences via the Strategic Priority Research Program (No. XDB23040000), Key Research Program of Frontier Sciences (No. QYZDJ-SSW-SYS024), and the External Cooperation Program of BIC (No. 114332KYSB20160007).

ORCID iDs

Zhi-Ping Jin  <https://orcid.org/0000-0003-4977-9724>

Hao Wang  <https://orcid.org/0000-0002-0556-1857>

Yuan-Zhu Wang  <https://orcid.org/0000-0001-9626-9319>

Fu-Wen Zhang  <https://orcid.org/0000-0002-5936-8921>

Yuan-Chuan Zou  <https://orcid.org/0000-0002-5400-3261>

Yi-Zhong Fan  <https://orcid.org/0000-0002-8966-6911>

Da-Ming Wei  <https://orcid.org/0000-0002-9758-5476>

References

- Abadie, J., Abadie, J., Abbott, B. P., et al. 2010, *CQGra*, **27**, 173001
- Abbott, B. P., Abbott, R., Abbott, T. D., et al. (LIGO Scientific Collaboration) 2016, *ApJL*, **832**, L21
- Abbott, B. P., Abbott, R., Abbott, T. D., et al. (LIGO Scientific Collaboration) 2017, *PhRvL*, **119**, 161101
- Aloy, M. A., Janka, H.-T., & Müller, E. 2005, *A&A*, **436**, 273
- Baiotti, L., & Rezzolla, L. 2017, *RPPH*, **80**, 096901
- Barnes, J., & Kasen, D. 2013, *ApJ*, **773**, 18
- Barthelmy, S. D., Barbier, L. M., Cummings, J. R., et al. 2005, *SSRv*, **120**, 143
- Barthelmy, S. D., Baumgartner, W. H., Beardmore, A. P., et al. 2015, GCN Circ, **17761**, 1
- Baumgartner, W. H., Tueller, J., Markwardt, C. B., et al. 2013, *ApJS*, **207**, 19
- Beardmore, A. P., Page, K. L., Palmer, D. M., & Ukwatta, T. N. 2015, GCN Circ, **17743**, 1
- Berger, E. 2014, *ARA&A*, **52**, 43
- Berger, E., Fong, W., & Chornock, R. 2013, *ApJL*, **744**, L23
- Berger, E., Kulkarni, S. R., Pooley, G., et al. 2003, *Natur*, **426**, 154
- Bromberg, O., Nakar, E., Piran, T., & Sari, R. 2013, *ApJ*, **764**, 179
- Burrows, D. N., Grupe, D., Capalbi, M., et al. 2006, *ApJ*, **653**, 468
- Butler, N., Watson, A. M., Kuttyrev, A., et al. 2015, GCN Circ, **17762**, 1
- Castro-Tirado, A. J., Sanchez-Ramirez, R., Lombardi, G., & Rivero, M. A. 2015, GCN Circ, **17758**, 1
- Clark, J., Evans, H., Fairhurst, S., et al. 2015, *ApJ*, **809**, 53
- Clark, J. P. A., & Eardley, D. M. 1977, *ApJ*, **215**, 311
- Coulter, D. A., Foley, R. J., Kilpatrick, C. D., et al. 2017, *Sci*, **358**, 1556
- Coward, D. M., Howell, E. J., Piran, T., et al. 2012, *MNRAS*, **425**, 2668
- Dai, Z. G., & Gou, L. J. 2001, *ApJ*, **552**, 72
- Dominik, M., Berti, E., Shaughnessy, R., et al. 2015, *ApJ*, **806**, 263
- Drout, M. R., Piro, A. L., Shappee, B. J., et al. 2017, *Sci*, **358**, 1570
- Eichler, D., Livio, M., Piran, T., & Schramm, D. N. 1989, *Natur*, **340**, 126
- Evans, P. A., Beardmore, A. P., Page, K. L., et al. 2009, *MNRAS*, **397**, 1177
- Fan, Y. Z., & Wei, D. M. 2011, *ApJ*, **739**, 47
- Fan, Y. Z., Wei, D. M., Zhang, F. W., & Zhang, B. B. 2012, *ApJ*, **751**, 49
- Fan, Y. Z., Yu, Y. W., Xu, D., et al. 2013, *ApJL*, **779**, L25
- Fong, W., & Berger, E. 2013, *ApJ*, **776**, 18
- Fong, W., Berger, E., Margutti, R., et al. 2012, *ApJ*, **756**, 189
- Fong, W., Berger, E., Margutti, R., & Zauderer, B. A. 2015, *ApJ*, **815**, 102
- Fong, W., Berger, E., Metzger, B. D., et al. 2014, *ApJ*, **780**, 118
- Frail, D. A., Kulkarni, S. R., Sari, R., et al. 2001, *ApJ*, **562**, L55
- Gehrels, N., Norris, J. P., Barthelmy, S. D., et al. 2006, *Natur*, **444**, 1044
- Goldstein, A., Veres, P., & Burns, E. 2017, *ApJL*, **848**, L14
- Golenetskii, S., Aptekar, R., Frederiks, D., et al. 2015, GCN Circ, **17752**, 1
- Gottlieb, O., Nakar, E., & Piran, T. 2017, arXiv:1705.10797
- Guetta, D., & Piran, T. 2005, *A&A*, **435**, 421
- Hotokezaka, K., Kyutoku, K., Tanaka, M., et al. 2013, *ApJL*, **778**, L16
- Huang, Y. F., Cheng, K. S., & Gao, T. T. 2006, *ApJ*, **637**, 873
- Jeong, S., Park, I. H., Hu, Y., et al. 2016, GCN Circ, **19847**, 1
- Jin, Z. P., Hotokezaka, K., Li, X., et al. 2016, *NatCo*, **7**, 12898
- Jin, Z. P., Li, X., Cano, Z., et al. 2015, *ApJL*, **811**, L22
- Jin, Z. P., Yan, T., Fan, Y. Z., & Wei, D. M. 2007, *ApJL*, **656**, L57
- Kann, D. A., Tanga, M., & Greiner, J. 2015, GCN Circ, **17757**, 1
- Kasliwal, M. M., Korobkin, O., Lau, R. M., Wollaeger, R., & Fryer, C. L. 2017a, *ApJL*, **843**, L34
- Kasliwal, M. M., Nakar, E., Singer, L. P., et al. 2017b, *Sci*, **358**, 1559
- Knust, F., Greiner, J., van Eerten, J. H., et al. 2017, arXiv:1707.01329
- Kochanek, C. S., & Piran, T. 1993, *ApJL*, **417**, L17
- Kouveliotou, C., Meegan, C. A., Fishman, G. J., et al. 1993, *ApJL*, **413**, L101
- Kulkarni, S. R. 2005, arXiv:astro-ph/0510256
- Kumar, P., & Granot, J. 2003, *ApJ*, **591**, 1075
- Kumar, P., & Zhang, B. 2015, *PhR*, **561**, 1
- Lamb, G. P., & Kobayashi, S. 2017, arXiv:1706.03000
- Lazzati, D., Deich, A., Morsony, B. J., & Workman, J. C. 2017, *MNRAS*, **471**, 1652
- Levan, A. J., Wiersema, K., Tanvir, N. R., et al. 2016, GCN Circ, **19846**, 1
- Li, L.-X., & Paczyński, B. 1998, *ApJL*, **507**, L59
- Li, X., Hu, Y. M., Fan, Y. Z., & Wei, D. M. 2016, *ApJ*, **827**, 75
- Li, X., Hu, Y. M., Jin, Z. P., Fan, Y. Z., & Wei, D. M. 2017, *ApJL*, **844**, L22
- Liang, E.-W., Yi, S.-X., Zhang, J., et al. 2010, *ApJ*, **725**, 2209
- Lien, A., Sakamoto, T., Barthelmy, S. D., et al. 2016, *ApJ*, **829**, 7
- Lien, A., Sakamoto, T., Gehrels, N., et al. 2014, *ApJ*, **783**, 24
- Lü, H. J., Zhang, H. M., Zhong, S. Q., et al. 2017, *ApJ*, **835**, 181
- Lü, J., Zou, Y.-C., Lei, W.-H., et al. 2012, *ApJ*, **751**, 49
- Malesani, D., Xu, D., Watson, D. J., Blay, P., et al. 2015, GCN Circ, **17756**, 1
- Mangano, V., Holland, S. T., Malesani, D., et al. 2007, *A&A*, **470**, 105
- Marshall, F. E., & Beardmore, A. P. 2015, GCN Circ, **17751**, 1
- Meegan, C., Lichti, G., Bhat, P. N., et al. 2009, *ApJ*, **702**, 791
- Melandri, A., D'Avanzo, P., D'Elia, V., et al. 2015, GCN Circ, **17760**, 1
- Metzger, B. D., Martínez-Pinedo, G., Darbha, S., et al. 2010, *MNRAS*, **406**, 2650
- Murguía-Berthier, A., Ramirez-Ruiz, E., Montes, G., et al. 2017, *ApJL*, **835**, L34
- Nagakura, H., Hotokezaka, K., Sekiguchi, Y., Shibata, M., & Ioka, K. 2014, *ApJL*, **784**, L28
- Nakar, E. 2007, *PhR*, **442**, 166
- Nicuesa Guelbenzu, A., Klose, S., Rossi, A., et al. 2011, *A&A*, **531**, L6
- Paczynski, B. 1990, *ApJ*, **363**, 218
- Palmer, D. M., Barthelmy, S. D., & Cummings, J. R. 2016, GCN Circ, **19844**, 1
- Paschalidis, V. 2017, *CQGra*, **34**, 084002
- Perley, D. A., & McConnell, N. J. 2015, GCN Circ, **17745**, 1
- Petrillo, C. E., Dietz, A., & Cavaglià, M. 2013, *ApJ*, **767**, 140
- Pian, E., D'Avanzo, P., Benetti, S., et al. 2017, *Natur*, **551**, 67
- Piran, T. 2004, *RvMP*, **76**, 1143
- Planck Collaboration, Ade, P. A. R., Aghanim, N., Armitage-Caplan, C., et al. 2014, *A&A*, **571**, 16
- Rhoads, J. E. 1999, *ApJ*, **525**, 737
- Rossi, E., Lazzati, D., & Rees, M. J. 2002, *MNRAS*, **332**, 945
- Rybicki, G. B., & Lightman, A. P. 1979, *Radiative Processes in Astrophysics* (New York: Wiley)
- Sari, R., Piran, T., & Halpern, J. P. 1999, *ApJL*, **519**, L17
- Schlaflly, E. F., & Finkbeiner, D. P. 2011, *ApJ*, **737**, 103
- Siegel, M. H., Barthelmy, S. D., Burrows, D. N., et al. 2016, GCN Circ, **19833**, 1
- Sielles, K., Boer, M., Gendre, B., & Regimbau, T. 2016, arXiv:1606.03043
- Soderberg, A. M., Berger, E., Kasliwal, M., et al. 2006, *ApJ*, **650**, 261
- Stanbro, M., & Meegan, C. 2016, GCN Circ, **19843**, 1
- Stratta, G., D'Avanzo, P., Piranomonte, S., et al. 2007, *A&A*, **474**, 827
- Tanaka, M., & Hotokezaka, K. 2013, *ApJ*, **775**, 113
- Tanaka, M., Hotokezaka, K., Kyutoku, K., et al. 2014, *ApJ*, **780**, 31
- Tanvir, N. R., Levan, A. J., Fruchter, A. S., et al. 2013, *Natur*, **500**, 547
- Tanvir, N. R., Levan, A. J., Fruchter, A. S., et al. 2015, GCN Circ, **18100**, 1
- Tanvir, N. R., Levan, A. J., González-Fernández, C., et al. 2017, *ApJL*, **848**, L27
- Troja, E., Piro, H., van Eerten, H., et al. 2017, *Natur*, **551**, 71
- Troja, E., Sakamoto, T., Cenko, S. B., et al. 2016a, *ApJ*, **827**, 102
- Troja, E., Tanvir, N., Cenko, S. B., et al. 2016b, GCN Circ, **20222**, 1
- Villasenor, J. S., Lamb, D. Q., Ricker, G. R., et al. 2005, *Natur*, **437**, 855
- Wang, Y. Z., Huang, Y. J., Liang, Y. F., et al. 2017, *ApJL*, **851**, L20
- Wei, D. M., & Jin, Z. P. 2003, *A&A*, **400**, 415
- Williamson, A. R., Biwer, C., Fairhurst, S., et al. 2014, *PhRvD*, **90**, 122004
- Woosley, S. E., & Bloom, J. S. 2006, *ARA&A*, **44**, 507
- Wu, X. F., Dai, Z. G., Huang, Y. F., & Lu, T. 2005, *MNRAS*, **357**, 1197
- Xu, D., Malesani, D., de Ugarte Postigo, A., et al. 2016, GCN Circ, **19834**, 1
- Xu, D., Starling, R. L. C., Fynbo, J. P. U., et al. 2009, *ApJ*, **696**, 971
- Yang, B., Jin, Z. P., Li, X., et al. 2015, *NatCo*, **6**, 7323
- Zhang, B., Dai, X., Lloyd-Ronning, N. M., & Mészáros, P. 2004, *ApJL*, **601**, L119
- Zhang, B., & Mészáros, P. 2002, *ApJ*, **571**, 876
- Zhang, B., & Mészáros, P. 2004, *IJMPA*, **19**, 2385
- Zhang, F.-W., Shao, L., Yan, J.-Z., & Wei, D.-M. 2012, *ApJ*, **750**, 88
- Zhang, S., Jin, Z. P., Wang, Y. Z., & Wei, D. M. 2017, *ApJ*, **835**, 73